Path-integral seismic imaging

E. Landa,[1]* S. Fomel[2] and T.J. Moser[3]

[1]*OPERA, Bat. IFR, Rue Jules Ferry, 64000 Pau, France,* [2]*Bureau of Economic Geology, University of Texas, Austin, Texas, USA, and*
[3]*Zeehelden Geoservices, van Alkemadelaan 550 A, 2597 AV 's-Gravenhage, The Netherlands*

ABSTRACT

A new type of seismic imaging, based on Feynman path integrals for waveform modelling, is capable of producing accurate subsurface images without any need for a reference velocity model. Instead of the usual optimization for traveltime curves with maximal signal semblance, a weighted summation over all representative curves avoids the need for velocity analysis, with its common difficulties of subjective and time-consuming manual picking. The summation over all curves includes the stationary one that plays a preferential role in classical imaging schemes, but also multiple stationary curves when they exist. Moreover, the weighted summation over all curves also accounts for non-uniqueness and uncertainty in the stacking/migration velocities. The path-integral imaging can be applied to stacking to zero-offset and to time and depth migration. In all these cases, a properly defined weighting function plays a vital role: to emphasize contributions from traveltime curves close to the optimal one and to suppress contributions from unrealistic curves. The path-integral method is an authentic macromodel-independent technique in the sense that there is strictly no parameter optimization or estimation involved. Development is still in its initial stage, and several conceptual and implementation issues are yet to be solved. However, application to synthetic and real data examples shows that it has the potential for becoming a fully automatic imaging technique.

INTRODUCTION

First, we set aside seismic velocities and work in a macromodel-independent context. A detailed and accurate velocity is usually seen as a precondition for obtaining an optimally focused seismic image of the subsurface of the earth. A common approach to velocity estimation is to formulate a criterion to quantify the degree of focusing and from there to derive a mechanism to update velocities. Examples of such criteria are a maximal signal semblance in zero-offset imaging or flatness in common-image gathers (CIG) for time or depth migration. Key to such techniques is the picking of important seismic events in prestack gathers, either manually or by an automatic procedure. Manual picking is both time consuming and subjective. Automatic picking is practical and useful in many situations (Fomel 2003; Stinson *et al.* 2004), but there

are cases where picking a single event is not sufficient to determine a unique velocity. Complicated wave-propagation effects, such as multiple reflections, mode conversions and wavefront triplications, can often cause serious problems for the assumptions underlying the velocity-analysis technique. For instance, picking a wrongly identified event may lead to velocities drifting away from realistic values during the velocity updating process.

A more fundamental problem in velocity estimation is related to the stochastic nature of the subsurface velocity, which is more properly represented in terms of probability density functions of velocities, rather than of one unique deterministic value (Jedlicka 1989). In other words, a single correct velocity model generally does not exist, but rather, if we take non-uniqueness and uncertainty into account, a collection of many models, which are all useful for obtaining a focused image. Deterministically, there are also objections to working with a single, supposedly optimal, velocity model. In stacking to

*E-mail: evgeny.landa@univ-pau.fr

zero-offset, an exact normal-moveout (NMO) velocity or stacking velocity may not exist, due to lateral variations. In prestack migration, it is not, *a priori*, clear from the prestack data which detail or resolution velocities can, or indeed should, be recovered for an optimal image. The migration velocity may not be identical to the interval velocity at all length scales and therefore may not be physically meaningful.

For these reasons, several macromodel-independent imaging techniques have been proposed in recent years. In practical implementations, these proposed methods differ considerably in the degree to which they are genuinely model-independent. An important class of methods is formed by multifocusing (MF, Gelchinsky *et al.* 1999a, Gelchinsky *et al.* 1999b) and the common-reflection-surface stack (CRS, Jäger *et al.* 2001). Multifocusing and CRS both estimate a set of kinematic wavefront attributes, with minimal assumptions about the subsurface velocity, to obtain an optimal zero-offset stacked section. However, they do not provide a seismic depth- or time-migrated image, at least not directly. Also, it may be argued that MF and CRS are still parameter-optimization approaches and, by re-parametrization (from wavefront attributes to stacking velocities), velocity-estimation techniques in disguise. A different approach, based on inverse scattering, was developed by Weglein *et al.* (2000), which has the potential of providing a subsurface image without a defined velocity.

We introduce and develop further a heuristic technique to obtain a subsurface image without specifying a velocity model, by using a path-integral approach. This means that we set aside not only the concept of a velocity, but also the stationary-phase approximation in wave modelling. Path integrals have recently been introduced in seismic wave modelling, in analogy to Feynman's path integrals in quantum mechanics (Lomax 1999; Schlottmann 1999). The path-integral method constructs the wavefield by summation over the contributions of elementary signals (wave functions in quantum mechanics) propagated along a representative sample of all possible paths between the source and observation points. It does not rely on the representation of a seismic event travelling along only one path, derived from a stationary-phase approximation or from Fermat's principle. Instead, it represents the seismic wave as sampling a larger volume between the two points, including, at least in theory, the Fresnel zones of all orders (Born and Wolf 1959). All random trajectories between the source and receiver within this volume are, in principle, taken into account. The phase contribution for each path is defined by the Lagrangian of the system and the summation of all phase contributions constitutes the complete seismogram, by constructive and destructive interference. The formal mathematical definition of

a path integral is rather complicated, and requires an infinite-dimensional integration (Johnson and Lapidus 2000). We will not discuss these difficulties here, but will assume that our path integrals can be numerically evaluated by parametrizing the trajectories by a finite number of parameters. The forward wave modelling by path integrals in an assumed-known velocity model has been discussed in detail by Lomax (1999) and Schlottmann (1999).

As shown by Keydar (2004), Landa (2004), Keydar and Shtivelman (2005) and Landa *et al.* (2005), path integrals can also be used in the reverse process: to obtain a subsurface image without any velocity information. At first sight, it would seem that path integrals in an unknown or undefined velocity do not make sense, and even more, that an indiscriminate integration over arbitrary random trajectories does not yield a mechanism that would focus data into an image. Three additional conditions are therefore essential:

1 the integration is carried out over a representative sample of all possible trajectories;

2 the application of properly designed weighting factors;

3 the choice of a complex or real-valued phase function in the exponential of the path integral.

With regard to the first condition, the integration trajectories are defined in the time (data) domain, rather than in the depth (model) domain. By a proper parametrization of the trajectories, it can be ensured that they represent a sufficiently general sampling of the set of physically realizable traveltime curves. With regard to the second condition, weighting factors derived from well-known data-dependent functionals, such as signal semblance or flatness of CIG gathers, ensure that the path integrals are convergent and converge to the correct image. For the third condition, the choice of a complex or real-valued phase function is a conceptual one, which leads to an oscillatory or exponential weighting function and, as such, has strong implications for the implementation of path-integral imaging. Note that application of these conditions does not in any way compromise the assumption of absence of information on velocity. Also note that both weighting and the selection of a representative sample of all trajectories achieve the same effect: exclusion of unrealistic trajectories.

The path-integral imaging can be considered in both time and depth domain. We present three important applications: stacking to zero-offset, time migration and depth migration. In all cases, the path integral consists of an integration over many (all) trajectories, rather than an optimization for one single trajectory over which the data is finally to be stacked. For a stack to zero-offset, the path integral consists of an integration of prestack seismic data along all physically

possible stacking trajectories instead of only along a single hyperbola corresponding to the highest coherence (e.g. semblance) in the conventional zero-offset imaging (NMO/DMO stack, multifocusing, CRS). For prestack time migration (PSTM) or prestack depth migration (PSDM), path-integral imaging consists of an integration of elementary signals over all possible diffraction traveltime curves (hyperbolic and non-hyperbolic), instead of only along a single trajectory corresponding to the estimated migration velocity. The constructive and destructive interference of elementary signals contributed by each path/trajectory produces an image that converges towards the correct one, which is obtained by a stack/migration procedure using an optimal velocity. In this process, all coherent data events are stacked and/or imaged, so possibly unwanted signals (mode conversions, multiple reflections) should be filtered out during preprocessing (multiple attenuation, coherent noise reduction), just as with classical migration schemes.

We begin by presenting the path-integral stack to zero-offset, and then discuss the application on time and depth migration. Since it is our intention to show only the feasibility of imaging by path integrals, we will not concentrate on computational efficiency. For the present, we accept the fact that a proper implementation of path-integral imaging may be computationally intensive (especially for depth migration), and in this respect cannot compete with current imaging techniques. We believe, however, that truly velocity-independent imaging has distinct advantages, compared with imaging based on velocity estimation, and that a next generation of computing hardware will make it computationally more attractive (Feynman 1982; Aharonov 1999).

PATH-INTEGRAL ZERO-OFFSET APPROXIMATION

The process of stacking prestack data to zero-offset conveniently allows us to introduce and discuss path-integral imaging. Stacking operators play a very important role in seismic data processing and imaging, with the main purpose of improving the signal-to-noise ratio and interpretability; the zero-offset stack is also input to poststack migration. Improving the quality of stacked sections remains the focus of intensive research. Much effort has been directed towards improving the accuracy of the NMO correction, e.g. shifted hyperbola (de Bazelaire 1988), multifocusing stack (Gelchinsky *et al.* 1999a,b), common-reflection-surface stack (Jäger *et al.* 2001), etc. However, these efforts have been of little use in stacking procedures, mainly because of a need for a multiparameter

search (3–5 parameters in the 2D case and 8–13 parameters in the 3D case), which is both time-consuming and not robust.

The most common application is common-data-point (CDP) stacking. Let us represent a stack Q for zero-offset time t_0 and location x_0 in the form,

$$Q(t_0, x_0; \alpha) = \int dh \int dt U(t, h) \, \delta(t - \tau(x_o, t_o, h; \alpha)), \qquad (1)$$

where $U(t, h)$ is the recorded CDP gather for location x_0, and h is the offset to be summed over the measurement aperture. The quantity $\tau = \tau(x_0, t_0, h; \alpha)$ represents the time-integration path/trajectory, which is parametrized by a parameter α (the integration over t is only formal, due to the δ-function, but included for clarity). The conventional zero-offset stack is obtained by optimizing for α, i.e.

$$Q_O(t_0, x_0) = Q(t_0, x_0; \alpha_0), \qquad (2a)$$

where the subscript O denotes the conventional optimization with respect to α_0, and its optimal value is defined by

$$S[U(\tau(x_0, t_0, h; \alpha_0), h)] = Max \, \alpha \, S[U(\tau(x_0, t_0, h; \alpha), h)], \qquad (2b)$$

where S is a functional on the data U along the trajectory $\tau(x_0, t_0, h; \alpha_0)$. For simplicity, we take S as the semblance, and assume $S'(\alpha_0) = 0$ and $S''(\alpha_0) < 0$ (the prime denoting the derivative with respect to α). The choice of semblance is nonessential, and formulations with other data functionals are conceivable (e.g. differential semblance, which satisfies the same assumptions). In the discussion below on the relationship with quantum mechanics, S denotes action.

For a simple hyperbolic CDP stack, we have

$$\tau(x_0, t_0, h; \alpha) = \sqrt{t_0^2 + h^2/\alpha^2} = \sqrt{t_0^2 + h^2/v_{st}^2}, \qquad (3)$$

where the summation parameter α in (1) is equal to the stacking velocity v_{st} and the integration is carried out over the CDP gather $U(t, h)$. The stacking velocity is usually estimated by velocity analysis, maximizing a coherence measure (e.g. semblance) calculated along different traveltimes defined by (3). In the case of multifocusing or CRS imaging techniques, τ is defined by more complex equations (Gelchinsky *et al.* 1999a, Gelchinsky *et al.* 1999b; Jäger *et al.* 2001) and α becomes a vector of wavefront kinematic parameters. We denote such a multiparameter vector in boldface, $\boldsymbol{\alpha}$.

We now introduce a heuristic development using the idea of the path-summation method of quantum mechanics (Feynman and Hibbs 1965). In Feynman's path-integral approach, a particle does not have just a single history/trajectory as it would have in classical theory. Instead, it is assumed to follow every possible path in the space–time domain, and a

wave-amplitude and phase is associated with each of these histories (trajectories). Each path contributes a different phase to the total amplitude of the wave function or the probability of going from a point *A* to a point *B*. The phase of the contribution from a given path is equal to the action *S* for that path in units of the quantum of action $\hbar$ (Planck's constant). Let us define the path of the particle between two points, *A* and *B*, as a function of *t*, i.e. $x(t)$. Then the total amplitude of the wave function, or the total probability of the particle going from point *A* to point *B*, can be written as:

$$K(A, B) = \sum_{\text{all patins}} \varphi(x(t)), \tag{4a}$$

where

$$\varphi(x(t)) \sim \exp[iS(x(t))/\hbar] \tag{4b}$$

How does this quantum mechanic formulary behave in the classical physics case? It is not absolutely clear how only one classical trajectory will be singled out as the most important. From (4), it follows that all trajectories make the same contribution to the amplitude, but with different phases. The classical limit corresponds to the case when all the dimensions (mass, time interval, and other parameters) are so large that the action *S* is much greater than the constant $\hbar$ ($S/\hbar \to \infty$).

In this case, the phases $S/\hbar$ of each partial contribution cover a very wide angle range. The real part of the function φ is equal to the cosine of these angles and can assume negative and positive values. If we now change the trajectory by a very small amount, the change in action *S* will also be small in the classical sense, but not small compared to $\hbar$. These small trajectory changes will lead, in principle, to very large changes of the phase and to very rapid oscillations of cosine and sine. Thus if one trajectory gives a positive contribution, another trajectory may give a negative contribution, even if they are very close, and they cancel each other out.

On the other hand, for a trajectory with stationary action (Fermat's trajectory), small perturbations, in practice, do not lead to changes in the action *S*. All contributions from the trajectories in this area have close phases and they interfere constructively. Only the vicinity of this stationary trajectory contributes to the total amplitude and (4) for the classical case can be schematically written as

$$K(x_0(t)) = F(x_0(t)) \exp[iS(x_0(t))/\hbar], \tag{5}$$

where *F* is some smooth functional of the path $x(t)$, and $x_0(t)$ is the Fermat path with stationary action: $\nabla_x S = 0$. It is precisely

this mechanism: firstly summation and secondly cancellation for large $S/\hbar$, which can be profitably applied in forward and inverse seismic wave modelling. We note that (5) may be compared with expressions from asymptotic ray theory, where the solution of the wave equation is written as a smooth amplitude function multiplied by the exponential of a stationary traveltime. In our application to seismic imaging, the trajectory $x(t)$ is not defined in the model, but in the data domain.

We now introduce a heuristic construction, based on the path summation idea for seismic stacking to zero-offset without knowing or estimating the velocity model. Instead of stacking seismic data along only one time trajectory corresponding to the Fermat path (or stationary point trajectory), our construction involves summation over all possible time trajectories. In this case (2) can be written as

$$Q_W = \int d\alpha \, w(\alpha) Q(\alpha), \tag{6}$$

where α now represents all possible time trajectories, $w(\alpha)$ stands for weights of different contributions and the subscript *W* denotes the weighted path integral (here, and in the remainder of the section, we omit the arguments x_0 and t_0 for the functions *Q*, *w* and *S*, and assume that all relevant integrals are taken at a current (x_0, t_0) pair. As an example, we can stack the data along different time trajectories corresponding to different stacking velocities (equation 3). Alternatively, the time trajectories may be parametrized by other medium attributes (even including anisotropy parameters). In any case, we emphasize that the path summation formula (6) is radically different from the conventional optimization formula (2a,b). This is, in fact, the main idea of this paper.

Figure 1 illustrates the situation in simple geophysical terms. The CDP gather (main panel) is stacked along different time trajectories (solid lines on the top of the gather) corresponding to different parameters α in (6). One of them coincides with the trajectory corresponding to the correct stacking velocity. This is the single curve which is used in the classical stack. The path-integral stack consists of all individual stacks, summed up and weighted according to (6). The final zero-offset stacked trace is plotted to the right of the panel.

The weighting function $w(\alpha)$ in the weighted path integral (6) can be chosen in many different ways. In general, it should be designed in such a way that the contributions from unlikely paths, which are far away from the stationary path, are suppressed, while contributions from paths close to the stationary one are emphasized. Here, by the distance between trajectories, we mean some measure on the set of available curves: for a finite number of parameters α, this could be a

Figure 1 Path-integral stacking to zero-offset, schematically shown for one CDP. A conventional stack is performed over the optimal stacking velocity curve (solid line), the path-integral stack is performed over many curves (thin lines) which are not necessarily optimal.
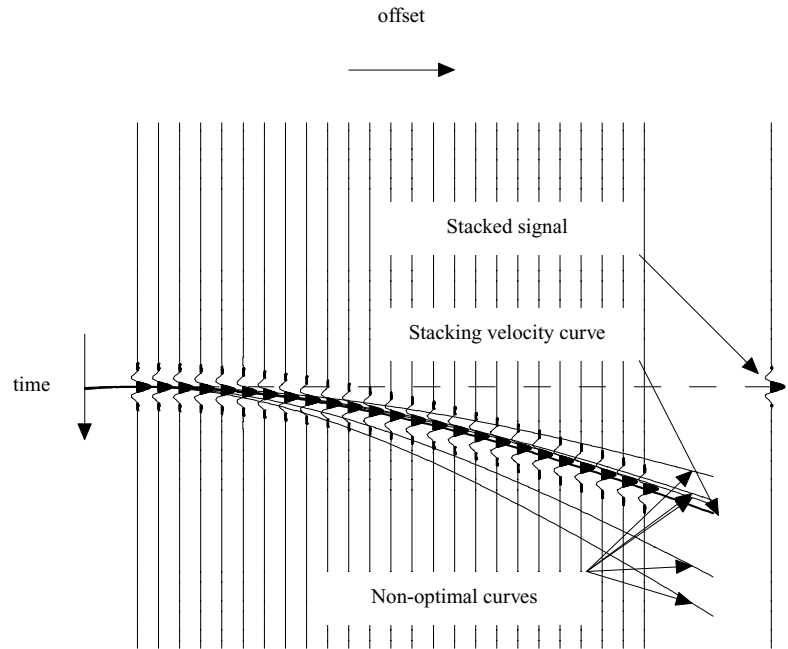
norm $||\alpha||$; for a single parameter, it could be $|\alpha|$. For the choice of a real-valued weighting function, the design should be such that its maxima correspond to the stationary points of $Q(\alpha)$. We may implicitly assume that the weighting functions are normalized, i.e. $\int d\alpha\, w(\alpha) = 1$, in order to enable true- or preserved-amplitude processing. In all cases, the integration runs over the relevant α-range.

There are several choices for the weighting function. If we choose an oscillatory weighting function,

$$Q_F = \int d\alpha \, \exp[i\beta S(\alpha)] Q(\alpha), \qquad (7)$$

where $S(\alpha)$ is the signal semblance, then (7) can be considered as a form of the Feynman path integral (4). The parameter β is a large positive number, which may serve as a control or bookkeeping parameter and plays the role of the inverse of Planck's constant. The above heuristic development deals with this type of weighting function. For an exponential weighting function,

$$Q_E = \int d\alpha \, \exp[\beta S(\alpha)] Q(\alpha), \qquad (8)$$

we have the Einstein–Smoluchovsky path integral, which was first introduced in the theory of Brownian motion (Einstein and Smoluchovsky 1997; Johnson and Lapidus 2000). Note that it only differs from (7) in that $i = \sqrt{-1}$ in the exponent of (7) is replaced by $+1$ in (8). However, both conceptually and numerically, the two integrals are quite different (see below).

A trivial choice is the Dirac-delta weighting function,

$$Q_D = \int d\alpha \, \delta(\alpha - \alpha_0) \, Q(\alpha) = Q(\alpha_0) = Q_0, \qquad (9)$$

for which the path-integral stacking (6) reduces to the classical limit and the conventional stack given by (2). However, for this case we would need to know α_0 (given by (2b)), which means we would have to optimize again for α. Instead, a weighting function $w(\alpha)$ which depends smoothly on α, as we are proposing here, does not require any optimization or precise knowledge of α_0. Optimization for α also implies a choice for a single optimum, whereas a smooth weighting function allows us to take several optima into account (conflicting dips), as well as the uncertainty in any optimal α.

It is straightforward to show that the path-integral stacks Q_F and Q_E approach the classical limit Q_O for $\beta \to \infty$ (in an asymptotical sense). For the Feynman path integral, this can be done by a stationary-phase approximation (Bleistein 1984; equation 2.7.18), under the assumptions $Q(\alpha) \to 0$ for $|\alpha - \alpha_0| \to \infty$, $S'(\alpha_0) = 0$ and $S''(\alpha_0) \neq 0$, i.e.

$$Q_F \approx \exp[i\beta S(\alpha_0) + i\mu\pi/4]\sqrt{\frac{2\pi}{\beta|S''(\alpha_0)|}}\, Q_0. \qquad (10)$$

Here, $Q_0 = Q(\alpha_0)$ is the classical stack (2a) and μ is the sign of $S''(\alpha_0)$. The stationary-phase approximation (10) shows that the Feynman path integral approaches the classical stack up to a complex factor.

A similar result holds for the Einstein path integral (de Bruijn 1959; equation 4.4.9), under the assumptions $S'(\alpha_0) = 0$ and $S''(\alpha_0) \neq 0$, i.e.

$$Q_E \approx \sqrt{\frac{-2\pi}{\beta S''(a_0)}} Q_0. \tag{11}$$

Again, the path-integral stack approaches the classical stack for $\beta \to \infty$ (up to a real factor in this case).

The numerical implementation of the path integrals with oscillatory and exponential weighting functions is quite different. The implementation of the Feynman path integral (7) requires a complicated mathematical apparatus, which is beyond the scope of this paper. Among the difficulties are:

1 the choice of integration limits;

2 the choice of a proper value for the parameter β in relation to $S(\alpha)$ and its derivatives;

3 the integration step size.

On the other hand, the Einstein path integral (8) has real contributions which decay rapidly as β and $|\alpha - \alpha_0|$ increase; as a result, it can be much more easily represented by a finite sum over a finite, realistic integration range. The differences are illustrated in Fig. 2, for one particular (x_0, t_0) pair and as a function of the single path parameter α. For a single parameter α, the implementation of the oscillatory integral (7) may still be tractable, but for paths parametrized by more than one parameter α, as in depth migration (see next section), a multidimensional integration is needed, and implementation issues can become critical. In any case, it is obvious that an adequate sampling of the α-space depends on the width of the integrand in (6) (the part where it is effectively non-zero), which in turn depends on the control parameter β. For very large values of β, an adequate sampling would require knowledge of the optimum α_0, which is undesirable for reasons made clear above.

Figures 3(a,b,c) shows a synthetic example of stacking to zero-offset. In Fig. 3(a) a synthetic zero-offset section is displayed (extracted from a prestack set obtained by Kirchhoff modelling on the upper part of a Marmousi-type model with an added water layer). Figure 3(b) shows the conventional stack, obtained by applying (2a) and (2b): for each x_0 and t_0, the stack is obtained by maximizing the semblance over a hyperbolic stacking curve (3). Figure 3(c) shows the Feynman path-integral stack, obtained by evaluating the path integral given by (7); we used 200 trajectories/velocities in this example. It is clear that the stacks are very similar and differ only in numerical detail. We emphasize, however, that the stack in Fig. 3(c) has been obtained in a fully automatic fashion.

Figure 4(a) shows a real data stack, obtained by conventional stacking; Fig. 4(b) shows the same data, stacked by Feynman path integration. Here, the Feynman path-integral stack shows much better fault planes, expressed by conflicting dips (in the upper part of the section). This is due to the integration over different trajectories for the same t_0; they include two stationary trajectories, one for the reflection off the sedimentary layer and one for the fault reflection. In this sense, the path-integral stacking has a similar effect as dip-moveout (DMO) processing.
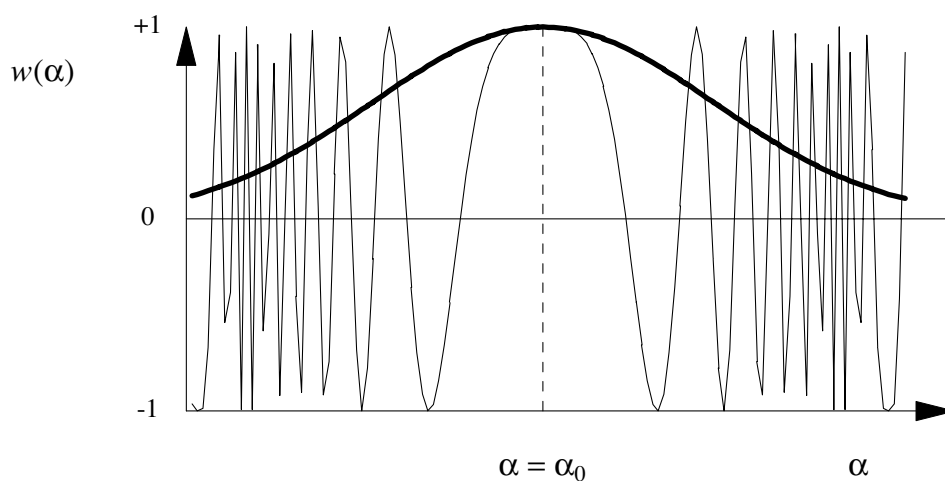

Figure 2 Path-integral weighting functions, exponential (thick) and oscillating (thin). The dashed line corresponds to the optimal value α_0 used in the classical limit.
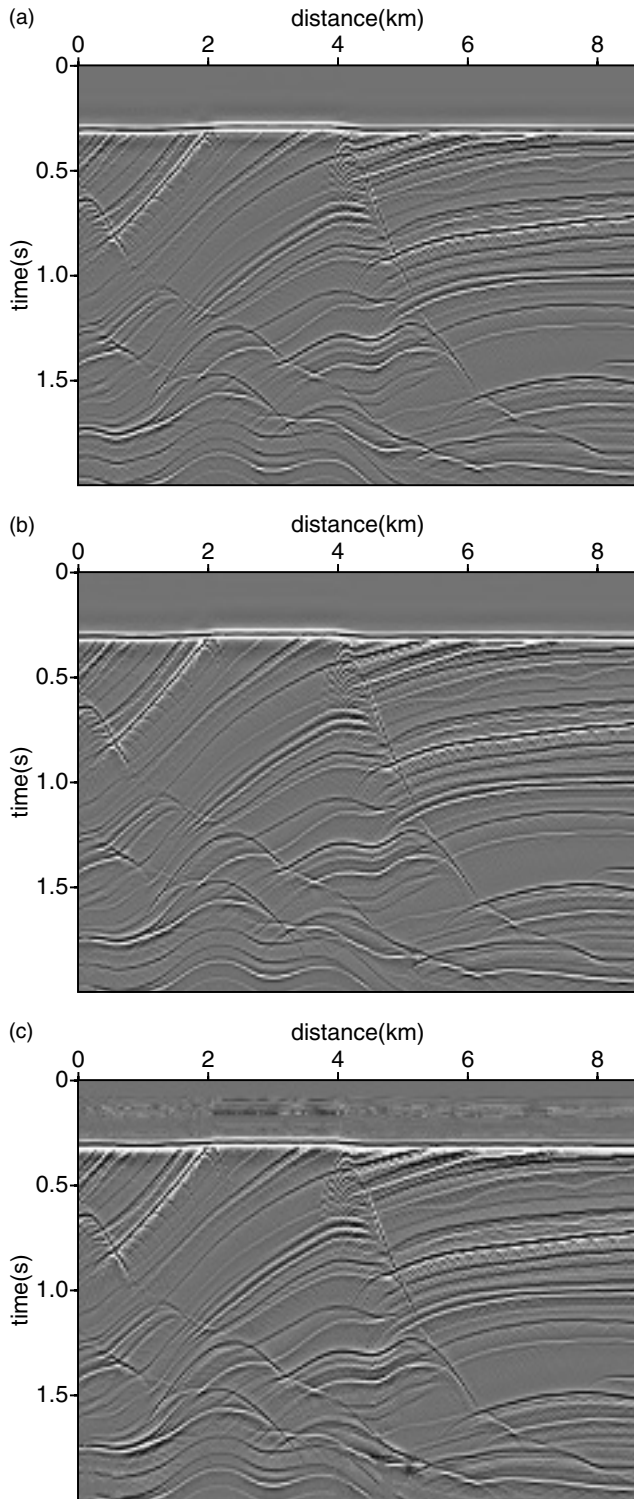
(a)

(b)

(c)

Figure 3 (a) Synthetic zero offset section; (b) zero-offset section obtained by optimal conventional stack; (c) zero-offset section obtained by Feynman path integral stack.
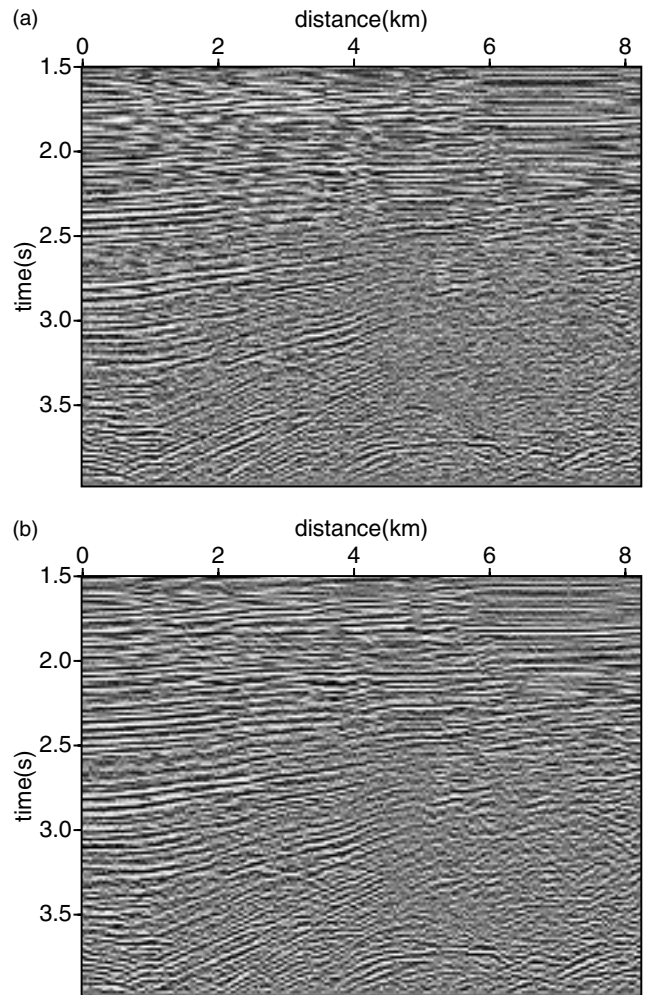

(a)

(b)

Figure 4 (a) Real-data zero-offset section obtained by optimal conventional stack; (b) real-data zero-offset section obtained by Feynman path-integral stack.

PATH-INTEGRAL TIME AND DEPTH MIGRATION

Migration can also be considered as a stacking procedure, and we can directly apply most of the ideas in the previous section. Migration velocity analysis can become non-trivial and a time-consuming part of prestack migration, particularly in depth. Let us consider the classical diffraction stack V_O for a subsurface location x in the form:

$$V_0(x) \sim \int d\xi \int dt \, U(t, \xi) \, \delta(t - t_d(\xi, x; \alpha_0)), \tag{12}$$

where $\mathbf{x}$ corresponds to (t_0, x) for time migration and to (z, x) for depth migration, $U(t, \xi)$ is the recorded input seismic data

for an arbitrary source–receiver configuration parametrized by the vector ξ, α_0 are the optimal summation path parameters (related to migration velocity), and t_d is the summation path over the diffraction traveltime curve (the kinematic part of the Green's function) corresponding to this migration velocity. The data configuration vector ξ is integrated over the measurement aperture, and the integration over time is only formal, but is included for clarity. Similarly to the conventional stacking procedure (equations 1 and 2), the conventional migration consists of finding an optimal migration velocity model, which results in diffraction curves along which the signal semblance is maximal. In the context of time migration, this requires us to find, for each (t_0, x), one or more parameters α that define an optimal hyperbolic, or non-hyperbolic, diffraction curve. For depth migration, it requires us to find a single velocity model parametrized by multiparameters α, such that the predicted traveltime curve for each (z, x) is optimal.

Following the path-integral concept introduced above, we consider a set of possible time trajectories t_d corresponding to a set of possible velocity models α, and use these trajectories for migration image construction. Again we do not optimize for the multiparameters α, but integrate over a representative range of α. The integration is weighted by a weighting function which is designed to attenuate contributions from unlikely trajectories and emphasize contributions from trajectories close to the optimal one. In this case (12) can be written as follows:

$$V_W(x) \sim \int d\alpha\, w(\alpha, x) \int d\xi \int dt\, U(t, \xi)\, \delta(t - t_d(\xi, x; \alpha)) \quad (13)$$

where t_d represents all possible time trajectories (dependent on α), $w(\alpha, x)$ denotes the weighting factor and α is integrated over all possible values of migration velocity. Here, $V_W(x)$ is our weighted path-integral migrated image. Again, several choices are possible for the weighting function $w(\alpha, x)$, i.e. the Feynman/oscillatory function (as in (7)), or the Einstein/exponential function (as in (8)). The Dirac-delta weighting function (9) reduces the path integral to the classical diffraction stack for optimal $\alpha = \alpha_0$.

The weighting function in migration can be derived from CIGs, where flatness of migrated events indicates a correct migration velocity, and curvature is proportional to velocity errors. Defining a flatness index p representing residual curvature calculated for each sample of the CIG ($p = 0$ for a
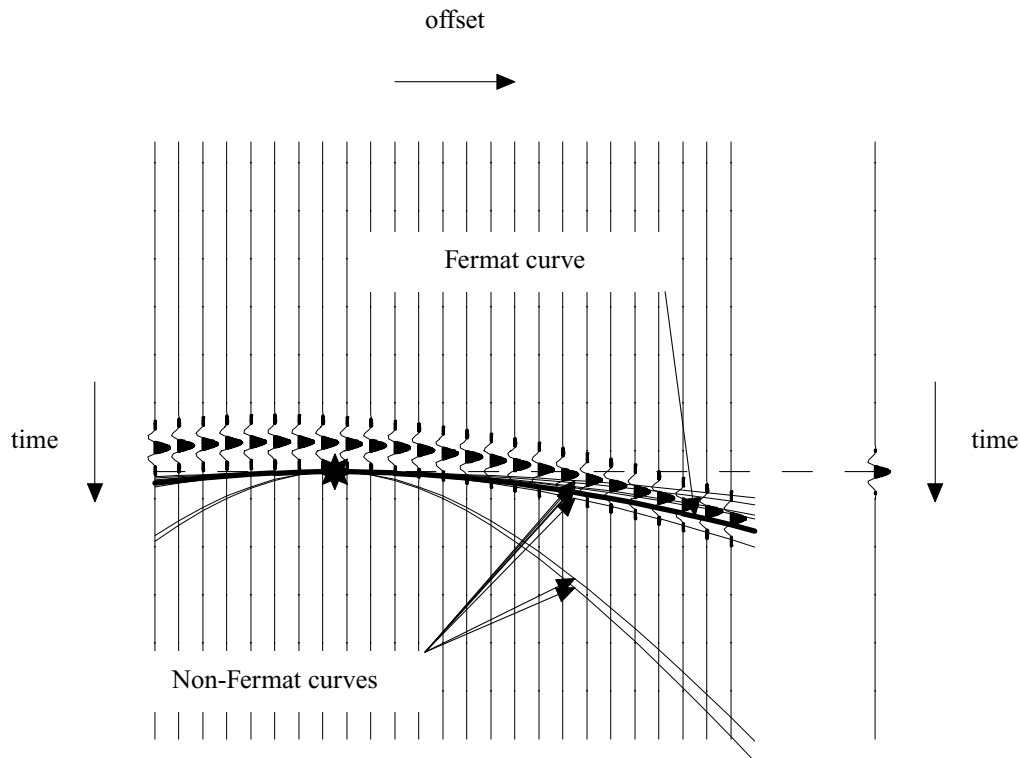
offset

Figure 5 Path-integral time migration for one shot gather. Conventional time migration attempts to find a traveltime trajectory for which the semblance is stationary (Fermat curve), path-integral time migration is a weighted integral over many (possibly non-stationary) curves.

flat event, $p \neq 0$ is proportional to the residual curvature), we construct an exponential weighting function as follows:

$$w(\boldsymbol{x}, \boldsymbol{\alpha}) \sim \exp[-|p(\boldsymbol{x}, \boldsymbol{\alpha})|]. \qquad (14)$$

This weighting function is of the Einstein/exponential type. The flatness measure plays the role of the action *S*. The evaluation of the weighted path integral (13) with (14) requires a multidimensional integration.

We first describe the application of the path-integral formalism to *prestack time migration*. The path-integral time migration is shown schematically in Fig. 5. The shot gather is stacked along all possible diffraction curves through one (x_0, t_0) pair. One curve coincides with the optimal semblance, and is used in the conventional migration (12). The path integral consists of all individual stacks, summed and weighted according to (13).

Figure 6(a) shows the path-integral time migration of part of the Sigsbee data set (Paffenholz *et al.* 2002). Here, we used the Feynman path integral with an oscillatory weighting function (with semblance as the data functional), and only hyperbolic traveltime trajectories. The path-integral migration succeeds in optimally imaging both flat and dipping reflectors, and also the target point-diffractors. For comparison, Fig. 6(b) shows the same path-integral migration, but using the Einstein path integral with an exponential weighting function (with CIG flatness as the data functional). It can be seen that it is smoother than Fig. 6(a), which is probably due to numerical integration artefacts of the Feynman path integral. On the other hand, the Feynman path-integral image has more continuous reflectors. We will not attempt a full explanation of these numerical differences between the Feynman and Einstein path-integral images in this paper, but leave it as a subject for further investigation.

A real data example (North Sea data, courtesy of Elf Aquitaine, Vaillant *et al.* 2000) is shown in Fig. 7. Figure 7(a) shows the conventional (optimized) time-migrated image, using the velocity continuation method (Fomel 2003), where the 2D migration velocity was estimated by slicing through the 3D velocity cube. Figure 7(b) shows path-integral time migration, obtained by weighted stacking along different traveltime trajectories, corresponding to a range of rms velocities of 1.4–3.0 km/s, and weights computed from the flatness of events in CIGs (see equation 14). The path-integral image is structurally very similar to the velocity continuation image, but it contains significantly fewer migration smiles, it has lower noise levels and it images the base of the salt better. Some loss in horizontal and vertical resolution for the path-integral images indicates
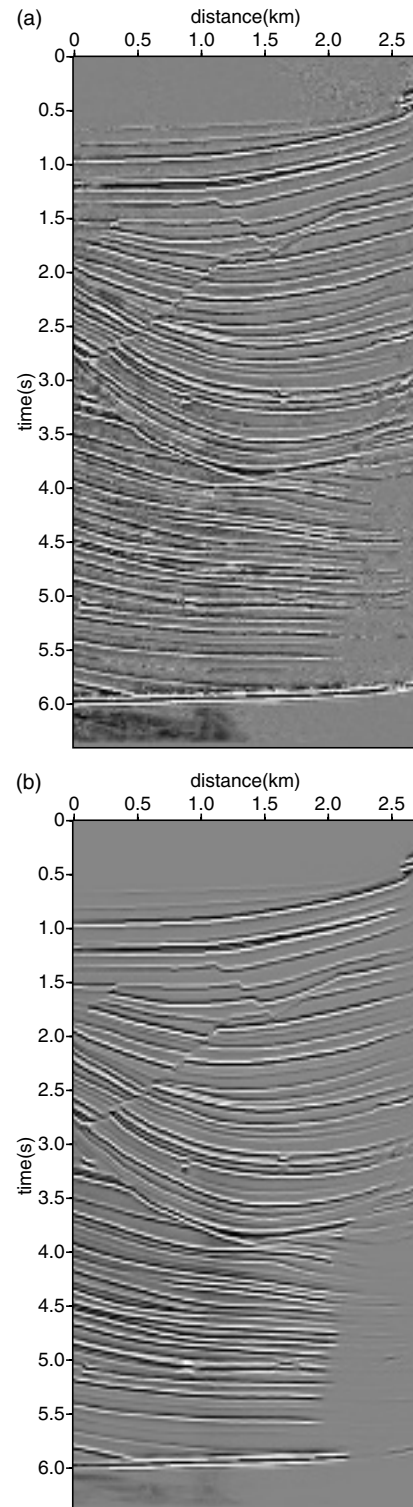

Figure 6 (a) Feynman path-integral time migration (oscillatory weighting function) of part of the Sigsbee data set; (b) Einstein path-integral time migration (exponential weighting function) of same data segment.
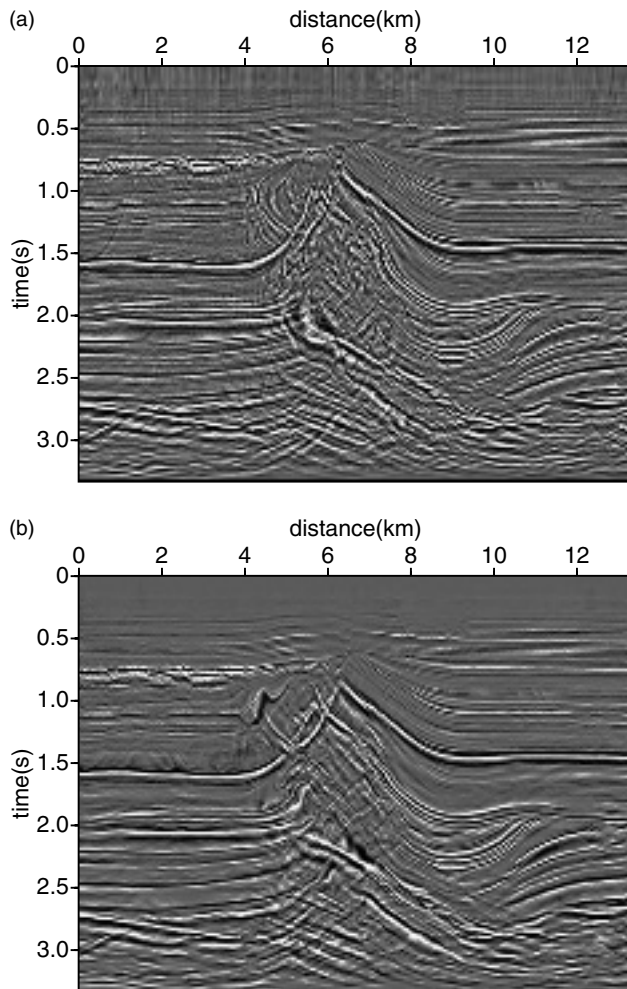
(a)

(b)

Figure 7 (a) Conventional (optimized) time-migrated image of North Sea data, obtained by velocity continuation; (b) path-integral time migrated image of North Sea data.

real physical resolution limits and should be attributed to uncertainties in velocities.

The same path-integral formalism can be applied to *prestack depth migration*. Figure 8 illustrates schematically the path-integral depth migration on a shot gather. The difficulty with depth migration, compared to time migration, is that, for a given traveltime trajectory passing through a datum point (x_0, t_0), it is not clear *a priori* where the stack should be located in depth. In addition, the traveltime trajectories in depth migration are often non-hyperbolic, so that multiparameters α are needed. In this paper, we construct physically realizable traveltime trajectories by repeated, local application of the eikonal equation for different random realizations of a velocity model. Note that this does not compromise on the model-independent

concept of path-integral imaging. It merely provides an effective selection of realizable traveltime trajectories and excludes unrealistic ones. In this context, we emphasize again that there is not necessarily a single final velocity model that results in an optimally focused image.

Figures 9–12 demonstrate the feasibility of path-integral depth migration on a relatively simple model, consisting of dipping and curved reflectors and strong velocity variations. Figure 9 shows the result of a conventional prestack depth migration for the correct velocity model. The traveltime trajectories were computed in 250 different realizations of randomly chosen velocity models, each one defined by linear interpolation from a regular grid of values. The traveltimes were used to produce CIGs. Figure 10 shows, for one particular velocity realization, the flatness index p corresponding to the curvature of reflection events on the CIGs. Values close to zero (grey in Fig. 10) indicate the flatness of CIG gathers and therefore the correct positioning of reflectors. The index is converted to a weight (equation 14) and shown in Fig. 11; here, black denotes correct positioning and white denotes either a low stack energy or poor positioning. Repeating this procedure for all velocity realizations and stacking the individual images with their weighting functions, we arrive at the path-integral depth image shown in Fig. 12. Note that the deepest reflector was imaged correctly, even although the correct velocity was not included in the suite of 250 test velocity models that we used to calculate the trajectories. This illustrates our argument that using random auxiliary velocity models does not contradict the model-independent concept of path-integral depth migration: a well-designed weighting function is capable of positioning the reflectors properly.

DISCUSSION AND CONCLUSIONS

The path-integral method allows reliable subsurface structural imaging without knowledge or selection of a velocity model, and therefore belongs to the class of macromodel-independent techniques. The usual step of migration velocity analysis, with its difficulties related to subjective and time-consuming manual velocity picking, can be avoided altogether. Path-integral seismic imaging can be considered as an authentic macromodel-independent technique, since it does not involve any optimization or estimation of parameters, representing traveltime trajectories or a velocity model.

Instead, the image is constructed by summation over many (ideally all) possible traveltime trajectories. It therefore allows the image to be fully dissociated from a reference model, thus
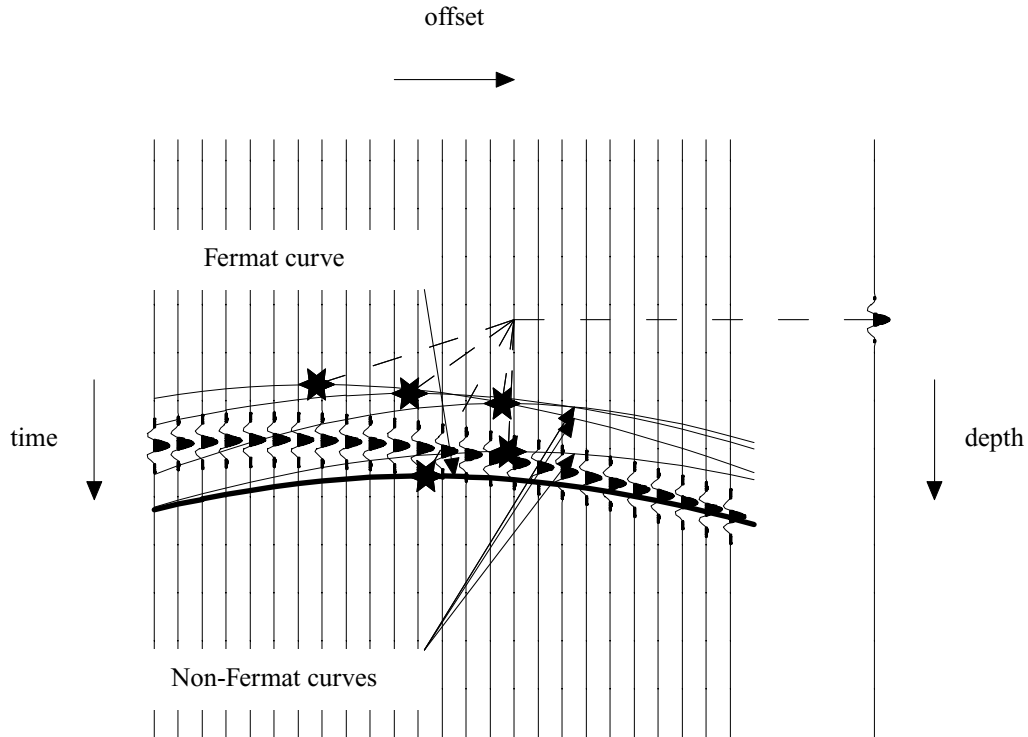
Figure 8 Path-integral depth migration. Weighted stacking occurs over trajectories calculated for many auxiliary random velocity models.
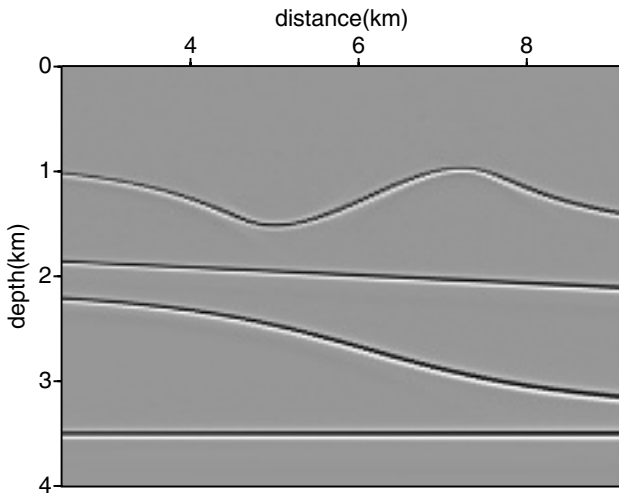

Figure 9 Conventional prestack depth migration in true velocity model (given by $v(x,z) = 1.5$ [km/s] $+ 0.5 + 0.36$ [s^{-1}]$(x + z)$.)
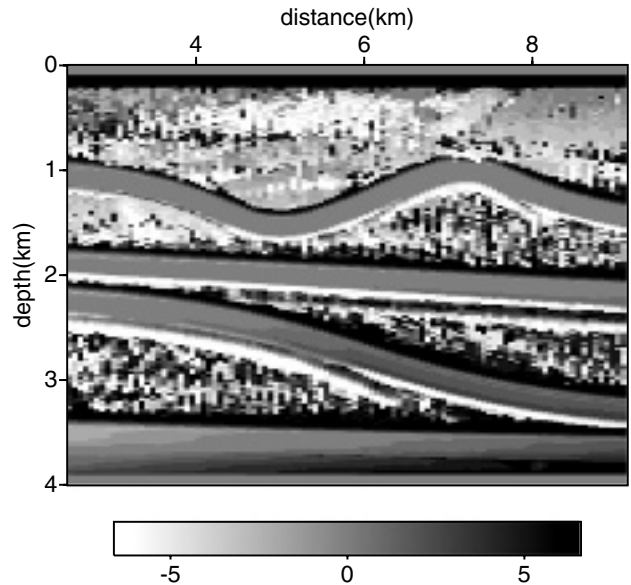

Figure 10 CIG curvature index for one individual velocity realization.

avoiding problems related to complicated wave propagation effects or resolution of different length scales.

The focusing mechanism is provided by data-defined weighting functions, which are designed to emphasize contributions from trajectories close to the optimal one and to suppress contributions from unlikely paths.

The path integral method can be applied to stacking to zero-offset, and time- and depth migration, and has the potential of becoming a fully automatic imaging technique. In all these cases, we may express the path-integral construction as follows:
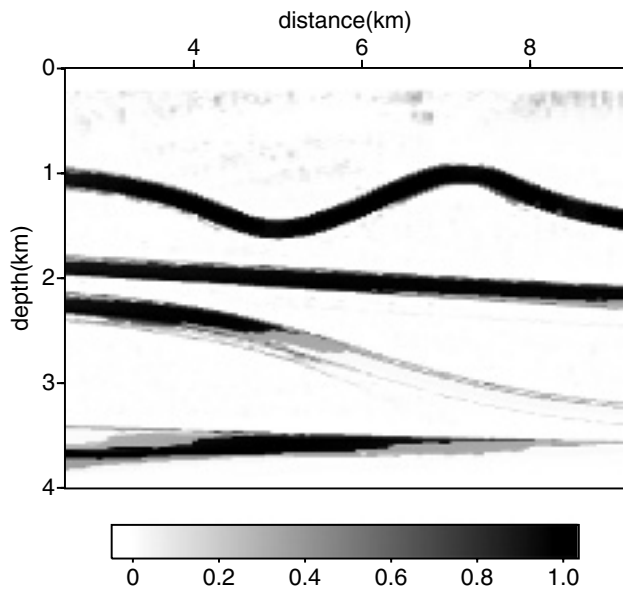
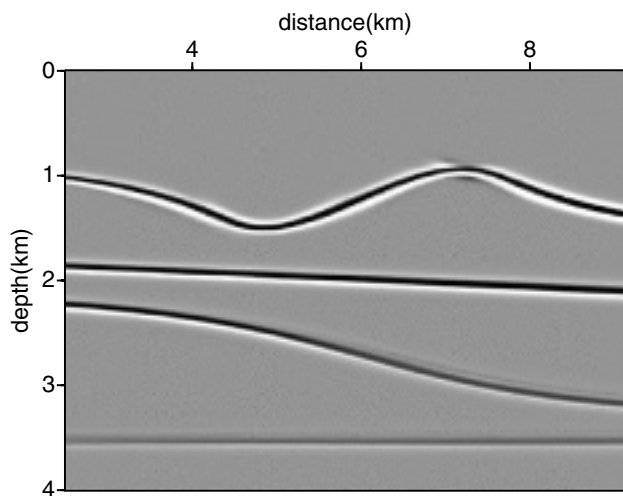**Figure 11** Weighting function derived from curvature index of Figure 10.

Figure 12 Path-integral depth-migrated image.

1 Choose an arbitrary model α (stacking velocity/trajectory in the case of a zero-offset stack, time-migration velocity curves for prestack time migration, a depth–velocity model for depth migration).

2 Perform the appropriate process: stack, time or depth migration, and then compute the weight.

3 Take another arbitrary model α, perform the appropriate process and add the weighted stack/image to the previous result.

4 Repeat step 3 until convergence.

Compare this procedure with the standard imaging procedure, which can be described by the same steps 1 and 2, but in step 3 a single stack/image with a weight exceeding all previous weights is chosen to replace a previous stack/image, and step 4 consists of repeating step 3 until all reasonable αs have been considered.

The path-integral imaging will be equal to this standard imaging procedure only in trivial situations of a single maximum weighting function. However, it may be different for complex models. The simplest example is zero-offset summation in the case of conflicting dips. A simple stack is unable to stack two events with different stacking velocities for the same t_0, but path integration can do this. For migration, if the weighting function (semblance or flatness) has local maxima for different models, conventional migration will construct the image using only one model (decided by the interpreter). Path integration will use all possible models which have stationary points for the weighting function and, moreover, it takes into account velocity (model) uncertainties.

The proposed path-integral scheme can be thus described in simple geophysical terms, related to the stationary-phase method. However, we opted for an exposition of the scheme in terms of quantum mechanics, not only because this may be intellectually appealing, but also to emphasize a deeper meaning, related to the fundamental uncertainty of the velocity model. In this sense, path integrals offer a non-classical approach to seismic imaging.

The implementation of path-integral imaging, at least in the stacking to zero-offset and time migration, is relatively simple, since the same system of nested loops as in the conventional process has to be traversed, but no velocity estimation is required. Several issues still need to be investigated: the implications of the choice of a weighting function (Feynman/oscillatory or Einstein/exponential); quality control of path-integral images; amplitude control (true-amplitude imaging); efficient implementation of path-integral depth imaging, among others. In any case, the application to synthetic and real data examples, both in time and in depth, shows the feasibility of the path-integral imaging method in complicated structural models.

ACKNOWLEDGEMENTS

encouragement. Tad Ulrych and two anonymous reviewers provided valuable suggestions that improved the quality of the paper.

REFERENCES

Aharonov D. 1999. *Noisy Quantum Computation*. PhD Thesis, Hebrew University, Jerusalem.

de Bazelaire E. 1988. Normal moveout revisited: inhomogeneous media and curved interfaces. *Geophysics* **53**, 143–157.

Bleistein N. 1984. *Mathematical Methods for Wave Phenomena*, Academic Press, Inc.

Born M. and Wolf E. 1959. *Principles of Optics*. Pergamon Press, Inc.

de Bruijn N.G. 1959. *Asymptotical Methods in Analysis*. Dover Publications, Inc.

Einstein A. and Smoluchovsky M. 1997. *Brownsche Bewegung. Untersuchungen über die Theorie der Brownschen Bewegung. Abhandlung über die Brownsche Bewegung und verwandte Erscheinungen,* Harri Deutsch, *(Reprint* **1905,** 1922).

Feynman R. 1982. Simulating physics with computers. *International Journal of Theoretical Physics* **21**, 467–488.

Feynman R. and Hibbs A. 1965. *Quantum Mechanics and Path Integrals*. McGraw–Hill Book Co.

Fomel S. 2003. Time-migration velocity analysis by velocity continuation. *Geophysics* **68**, 143–157.

Gelchinsky B., Berkovitch A. and Keydar S. 1999a. Multifocusing homeomorphic imaging, Part 1. Basis concepts and formulas. *Journal of Applied Geophysics* **42**, 229–242.

Gelchinsky B., Berkovitch A. and Keydar S. 1999b. Multifocusing homeomorphic imaging, Part 2. Multifold data set and multifocusing. *Journal of Applied Geophysics* **42**, 243–260.

Jäger R., Mann J., Höcht G. and Hubral P. 2001. Common-reflection-surface stack: Image and attributes. *Geophysics* **66**, 97–109.

Jedlicka J. 1989. *Stochastic normal moveout correction*. Stanford Exploration Project-60 report, 165–178.

Johnson G.W. and Lapidus M.L. 2000. *The Feynman Integral and Feynman's Operational Calculus*. Clarendon Press, Oxford.

Keydar S. 2004. Homeomorphic imaging using path integrals. 66th EAGE Conference, Paris, France, Extended Abstracts, P078.

Keydar S. and Shtivelman V. 2005. Imaging zero-offset sections using multipath summation. *First Break* **23**, 21–25.

Landa E. 2004. Imaging without a velocity model using path-summation approach. 74th SEG Meeting, Denver, USA, Expanded Abstracts, 1016–1019.

Landa E., Reshef M. and Khaidukov V. 2005. Imaging without a velocity model using path-summation approach: this time in depth. 67th EAGE Conference, Madrid, Spain, Extended Abstracts, P011.

Lomax A. 1999. Path-summation waveforms. *Geophysical Journal International* **138**, 702–716.

Paffenholz J., Stefani J., McLain B. and Bishop K. 2002. SIGSBEE_2A synthetic subsalt data set image quality as function of migration algorithm and velocity model error. 64th EAGE Conference, Florence, Italy, Extended Abstracts, B019.

Schlottmann R.B. 1999. A path integral formulation of acoustic wave propagation. *Geophysical Journal International* **137**, 353–363.

Stinson K.J., Chan W.K., Crase E., Levy S., Reshef M. and Roth M. 2004. Automatic imaging: velocity veracity. 66th EAGE Conference, Paris, France, Extended Abstracts, C018.

Vaillant L., Calandra H., Sava P. and Biondi B. 2000. 3-D wave-equation imaging of a North Sea dataset: Common-azimuth migration + residual migration. 70th SEG Meeting, Calgary, Canada, Expanded Abstracts, 874–877.

Weglein A., Matson K., Foster D., Carvalho P., Corrigan D. and Shaw S. 2000. Imaging and inversion at depth without a velocity model: theory, concepts and initial evaluation. 70th SEG Meeting, Calgary, Canada, Expanded Abstracts, 1016–1019.